Alternating Crack Propagation during Directional Drying

G. Gauthier,[†] V. Lazarus,*[,‡] and L. Pauchard[†]

FAST, CNRS UMR 7608, Université Paris Sud-11, bât. 502 Campus Universitaire, 91405 Orsay Cedex, France, and Université Pierre et Marie Curie-Paris 6, UMR 7190 (Institut Jean Le Rond d'Alembert), Boite courrier 161-162, 4 Place Jussieu, Paris F-75005, France

Received December 21, 2006. In Final Form: March 13, 2007

The propagation of fractures during the drying of a colloidal silica suspension confined in a vertical microtube is investigated. During the drying process, the particle concentration increases until gel formation. In the gelled region, the tensile stresses increase and lead to the formation of two vertical perpendicular cracks propagating in the drying direction, dividing the tube into four equivalent regions. Throughout the drying process, these two fractures do not propagate at the same velocity. The top crack inhibits the propagation of the crack that is left behind, and the slow propagation of a fracture is followed by the rapid propagation of the other.

Introduction

Understanding the formation and the dynamics of cracks is of fundamental and practical interest. On one hand, cracks can invade a surface with an apparent hierarchy.[1,2] Crack patterns induced by a drying process are common in muds and paints where successive generations of cracks divide a plane into polygonal domains.[3] Cracks appear in many coatings and material elaborations and generally need to be avoided. Also, crack morphologies have recently been investigated with the aim of both restoration and judging the authenticity of paintings.[4] On the other hand, cracks can propagate simultaneously into the volume of the medium, as is the case in many phenomena of geological interest such as the generation of basalt columns.[5,6] Because stresses induced by drying are similar to stresses that appear in the solidification of flow due to cooling,[7] the drying of corn starch is used to model columnar joints that appear in certain lava flows or basalt columns.[7−9] However, most of the studies on crack morphology deal with 2D problems such as the drying of layers[10−12] or suspensions confined between two parallel plates close to each other.[13−15] In these experiments, crack surfaces are not observable. In this letter, the 3D problem of drying dynamics and crack formation in a vertical capillary tube is studied. A colloidal gel exhibiting transparent, well-controlled physicochemical properties[16] is used, allowing us to study both the dynamics of cracks and their surface patterns. Figure 1 shows a self-organized structure composed of two vertical perpendicular cracks, each one following the direction of drying with an alternation of low and high velocities, yielding an alternation of rough and smooth crack surface patterns. The description and measurement of this alternating crack propagation scheme are presented in this paper.

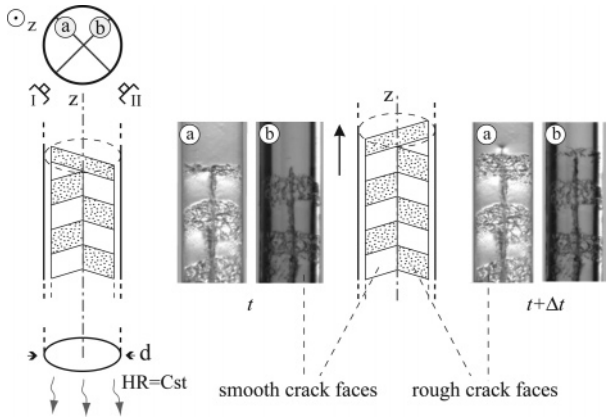

Figure 1. (Left) Vertical glass capillary of diameter ∼1 mm filled with a colloidal suspension; the single open edge allows for the evaporation of the solvent in surroundings maintained at a constant humidity rate (HR). On the two sketches corresponding to instants t and $t + \Delta t$, schematic illustrations of both cracks in vertical planes a and b that are perpendicular and intersect along the z axis are shown. (Right) Corresponding digitized images, taken by CCD cameras I and II, of the planar surfaces of these cracks (crack growth direction is given by the arrow; each image width is 1 mm).

Experiments and Results

Experiments are carried out, at room temperature, using aqueous suspensions of monodisperse silica particles (Ludox HS 40) of radius $r = 15 \pm 2$ nm and volume fraction $\phi \simeq 0.2$. In the absence of evaporation, the stability of the suspension is due to the competition between van der Waals attraction and electrostatic repulsion. To investigate unidirectional drying, a vertical glass capillary tube is used (Figure 1). Two CCD cameras, perpendicular to each other and to the tube axis (see sketch in Figure 1), allow the investigation of the dynamics of the process in the two perpendicular planes (a and b). Moreover, the tube can be rotated around its z axis to visualize the entire system at a given z position. The top of the tube is closed, and the bottom of the tube is placed in surroundings maintained at constant humidity using a desiccant. The tube is only partially filled with the suspension so that the air and solvent vapor, located above the suspension, can expand to compensate for the loss of solvent during desiccation. Among 12 similar experiments conducted on

* Corresponding author. E-mail: vlazarus@ccr.jussieu.fr.
[†] Université Paris Sud-11.
[‡] Université Pierre et Marie Curie-Paris 6.

(1) Atkinson, A.; Guppy, R. M. *J. Mater. Sci.* **1991**, *26*, 3869−3873.
(2) Groisman, A.; Kaplan, E. *Europhys. Lett.* **1994**, *25*, 415−420.
(3) Bohn, S.; Pauchard, L.; Couder, Y. *Phys. Rev. E* **2005**, *71*, 046214.
(4) Pauchard, L.; Lazarus, V.; Abou, B.; Sekimoto, K.; Aitken, G.; Lahanier, C. *Reflets Phys., Soc. Fr. Phys.* **2007**, *3*, in press.
(5) Ryan, M. P.; Sammis, C. G. *Geol. Soc. Am. Bull.* **1978**, *89*, 1295−1308.
(6) DeGraff, J. M.; Aydin, A. *Geol. Soc. Am.* **1987**, *99*, 600−617.
(7) Muller, G. *J. Geophys. Res.* **1998**, *103*, 15239−15253.
(8) Goehring, L.; Morris, S. W.; Lin, Z. *Phys. Rev. E* **2006**, *74*, 036115.
(9) Toramaru, A.; Matsumoto, T. *J. Geophys. Res.* **2004**, *109*, B02205.
(10) Lee, W. P.; Routh, A. F. *Langmuir* **2004**, *20*, 9885−9888.
(11) Tirumkudulu, M. S.; Russel, W. B. *Langmuir* **2004**, *20*, 2947−2961.
(12) Tirumkudulu, M. S.; Russel, W. B. *Langmuir* **2005**, *21*, 4938−4948.
(13) Allain, C.; Limat, L. *Phys. Rev. Lett.* **1995**, *74*, 2981−2984.
(14) Dufresne, E. R.; Corwin, E. I.; Greenblatt, N. A.; Ashmore, J.; Wang, D. Y.; Dinsmore, A. D.; Cheng, J. X.; Xie, X. S.; Hutchinson, J. W.; Weitz, D. A. *Phys. Rev. Lett.* **2003**, *91*, 224501.
(15) Dufresne, E.; Stark, D.; Greenblatt, N.; Cheng, J.; Hutchinson, J.; Mahadevan, L.; Weitz, D. *Langmuir* **2006**, *22*, 7144−7147.
(16) Brinker, C. J.; Scherer, G. W. *Sol-Gel Science: The Physics and Chemistry of Sol-Gel Processing*; Academic Press: Boston, 1990.

10.1021/la063702w CCC: $37.00
Published on Web 03/30/2007

tubes of diameter varying between $d = 0.9$ and 1.1 mm, 9 of them gave the observations described below. The failing of the other three to reproduce the same crack pattern may be due to the high sensitivity of the experiments to any manipulation during the drying process and to any bending of the tube.

As the sample loses solvent, one can notice the formation of two vertical cracks at the bottom of the tube that propagate upward. They expand in perpendicular planar surfaces (a and b), defined in Figure 1, and are therefore denoted cracks a and b. Observations using transmitted light allow a clear visualization of their motion. Figure 1 shows two images, taken by cameras I and II, of the vertical faces of cracks a and b, respectively. Each crack face displays an intriguing structure consisting of an alternation of smooth and rough appearance zones. These zones are shifted with half a period between cracks a and b. Qualitatively, the crack-growth process is the following. Cracks a and b nucleate in two perpendicular vertical planes containing the tube z axis. To understand the dynamics of propagation of these cracks, consider the situation where the two crack fronts are nearly at the same position along the z axis but one of the two, for instance, a, is slightly in front of crack b.[20] Crack a then propagates at a slow velocity, and it inhibits the propagation of crack b that is left behind, until this last one propagates rapidly and finally reaches and slightly passes the original crack (i.e., a). Then, crack b takes the place of crack a in the previous description. This process is repeated all along the capillary tube, leading to the fracture surfaces depicted in Figure 1. Rough surfaces correspond to the prints left by the slow velocity of the leading crack, and smooth ones correspond to the fast velocity of the crack catching up to the leading one.

To describe these patterns quantitatively, the dynamics of the process was studied by building spatio-temporal diagrams (Figure 2). Each spatio-temporal diagram corresponds to the time evolution of the light intensity of a single vertical line along the tube. Then, each describes the position of the crack tip in the z axis as a function of time. The advance displays a jerky motion whose average velocity, given by the dotted red line in Figure 2, is on the order of 40 nm/s. More precisely, suppose that at time $t = 0$ both crack fronts lie at $z = z_0$. Crack a then advances at the average rate following arrow 1 in Figure 2a, whereas crack tips b, setting back, do not propagate (arrow 1′ in Figure 2b). After a while, crack tips b reinitiate and propagate continuously and rapidly ($\sim 4\ \mu$m/s) 100 times faster than the average velocity until catching up to the top crack. This process is described by the vertical arrow (2′) in Figure 2b. Crack tips b reach the z_1 position of crack tips a and then pass it. At this point, crack b expands following the average rate: this is described by arrow 3′ in Figure 2b. At the same time, crack tip a, setting back, is stopped (arrow 2 in Figure 2a). This process is repeated with further reinitiation and then fast and slow propagation events.

This two-step, slow and fast, rough and smooth propagation set yields a quasi-periodic spatial structure along the crack faces. Figure 3 displays the evolution of its wavelength[21] λ (vertical length of a period) versus the distance z of the top of the period to the bottom of the tube (see Figure 2a for the definitions of λ and z). These measurements are made in a portion of the tube where the diameter is almost constant (less than 1% variation). One can notice that the wavelength increases before abruptly decreasing and then increasing again and so on. The decreasing parts coincide with the formation of secondary cracks perpendicular to cracks a and b. Such a horizontal transverse secondary crack is visible in Figure 2a and appears each four to seven periods. The location of the topmost secondary crack along the z axis is denoted z_I. In the inset, λ/d is plotted versus the nondimensional distance $(z - z_I)/d$ of the top of the period to the uppermost secondary crack. One can notice a good linear collapse of the points.

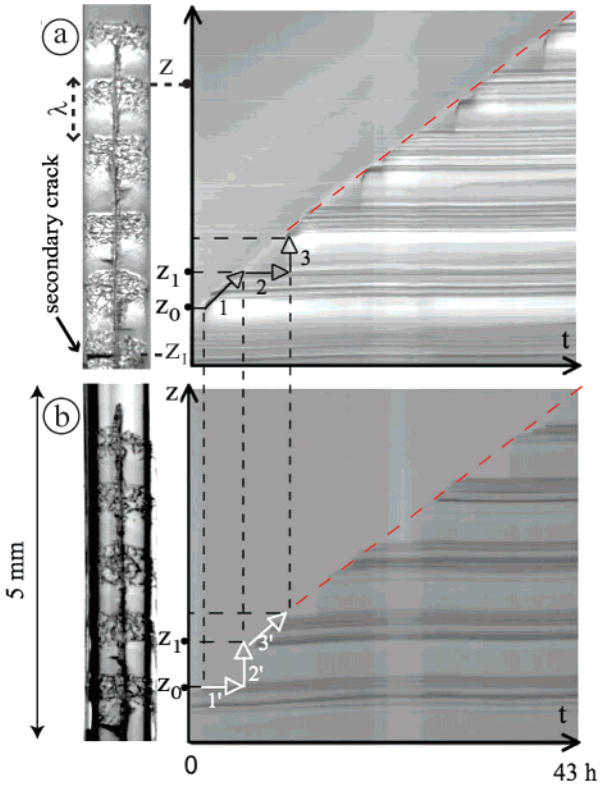

Figure 2. (Left) Digitized images taken in the final stage of the propagation of planar cracks a and b. (Right) Corresponding spatio-temporal diagrams describe the position of the crack tip on the z axis as a function of time for cracks a and b. The propagation of a planar crack is characterized by three stages: slow (1 or 3′), stop (2 or 1′), and fast (3 or 2′) expansions.

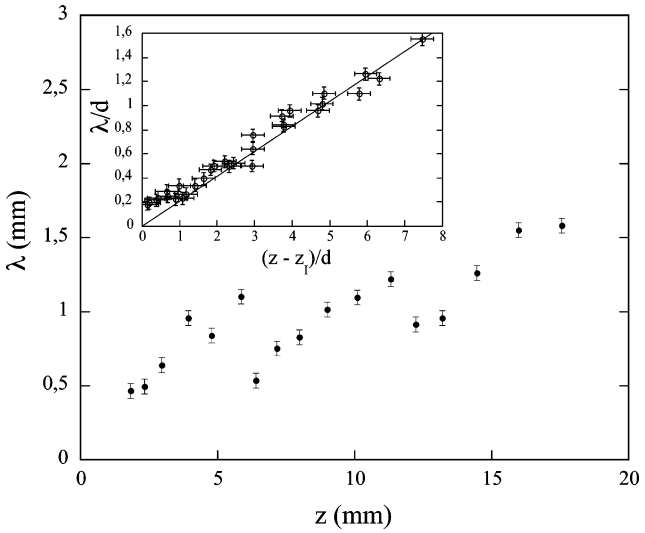

Figure 3. Typical wavelength evolution as a function of position z at the top of the period. In the inset, λ/d (d is the tube diameter) is plotted versus the distance $(z - z_I)/d$ to secondary transverse cracks for several tubes, (see Figure 2a for definitions of λ, z, and z_I).

Discussion

The experiments presented by Dufresne et al.[14] and those presented above are both directional drying experiments across

(17) Boeck, T.; Bahr, H. A.; Lampenscherf, S.; Bahr, U. *Phys. Rev. E* **1999**, *59*, 1408−1416.
(18) Gdoutos, E. E. *Fracture Mechanics Criteria and Applications*; Kluwer Academic: Dordrecht, The Netherlands, 1990.
(19) Hofmann, M.; Bahr, H. A.; Linse, T.; Bahr, U.; Balke, H.; Weiss, H. F. *Int. J. Fract.* **2006**, *141*, 345−356.
(20) Because crack a divides the tube along the diameter into two parts, planar surface b undergoes two independent cracks, one on each side of crack a. However, to lighten the writing, these two cracks are denoted as crack b here and in the sequel.
(21) Because this length is not constant, one shall rather speak about a pseudowavelength, but the term wavelength is kept in the text to lighten its discussion.

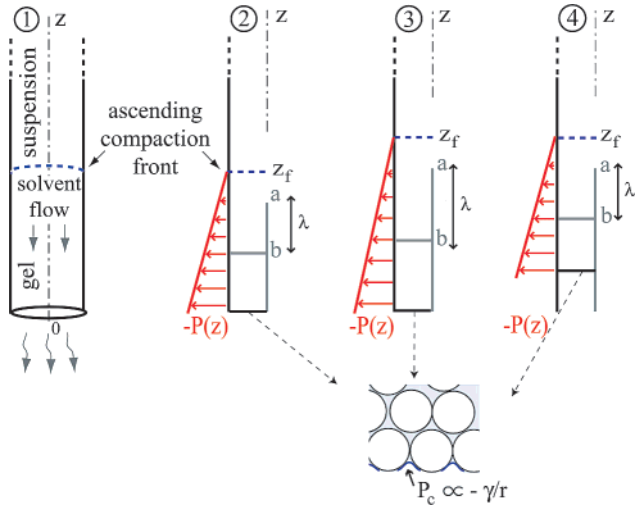

Figure 4. Underlying mechanism. (1) Coexistence of a suspension and gelled region delimited by the compaction front. (2) Vertical variation of the pressure in the gelled phase at time t. (3) At time $t' > t$, the pressure gradient decreases, hence the wavelength increases. (4) After the formation of a secondary horizontal crack forming a new air−water interface, the pressure gradient abruptly increases, hence the wavelength abruptly decreases.

one end of a capillary tube; only the geometry used is different: a flat tube in the first case and a circular tube used here. Therefore, let us adapt the mechanism that they validated for a colloidal suspension drying in flat capillary tubes to the drying in the cylindrical tubes used in our experiments. For this, suppose the existence of a compaction front, denoted z_f in Figure 4, delimiting the bottom gelled region and the top still liquid region. Suppose, moreover, that the gelled region is composed of a randomly packed monodisperse spheres matrix of constant porosity, filled with solvent. Because of the nanometric size of the particles, the solvent forms nanomenisci at the bottom air−gel interface (Figure 4). The pressure P_c at this interface[14,10] is $P_c - P_0 \propto -\gamma/r$, where r is the radius of the particles ($\gamma/r \approx 5 \times 10^6$ Pa for the air−water interface if $r = 15$ nm), but the top of the gelled region is at the atmospheric pressure $P_0 \approx 10^5$ Pa. This pressure gradient drives the solvent flow through the porous medium accordingly to Darcy's law. This flow carries silica particles to the compaction front so that the gel progressively invades the tube during the advancement of the compaction front. Supposing that the fluid flow resulting from this difference in pressure is uniform in each horizontal section and that the porosity of the gel is uniform, using the law of mass conservation for the fluid phase and Darcy's law, one realizes that $P(z) \approx P_c(z_F - z)/z_F$ (where $\rho gh \approx 10^3$ Pa $\ll P_0 \ll P_c$ has been used).

To explain the crack formation, let us propose the following explanation based on continuum mechanics. In the gelled region, the depression is not only responsible for the solvent transport through the porous network but also leads to high shrinkage stresses. However, shrinking is constrained by strong adhesion on the tube wall. This growing misfit results in increasing the internal tensile stresses. When the stresses exceed a threshold value, they are released by the formation of cracks that invade the gel. The dynamics of crack propagation shall be understood in the framework of linear elastic fracture mechanics using Griffith's criterion based on simple energy balance arguments:[17,18] the crack propagates when the energy release rate (energy released per unit of crack surface creation) exceeds a critical value. This release rate, which is specific to each crack, depends on the geometry and the energy stored in the solid matrix. On one hand, at fixed geometry, the stored energy increases as the compaction front advances. On the other hand, at fixed stored energy, the energy release rate of the leading crack is higher than at the rear crack because the loading of the rear crack is diminished by the presence of the traction-free surfaces of the leading crack near its front. Hence, the energy release rate evolves as the distance between the two cracks changes: it decreases or increases at the rear crack when the distance between the two cracks increases or decreases, respectively. These two statements can be coupled to understand the propagation pattern. The more loaded leading crack reaches the threshold and follows the compaction front (it cannot advance further because of the liquid region), but because of the increase in the distance between the cracks, the release rate of the crack left behind decreases. Meanwhile, the energy stored by drying increases enough that the propagation threshold of the rear crack is finally reached and the crack propagates. Now the geometric effect is in the other sense: the distance between the two cracks decreases so that the energy release rate of the rear crack increases and stays above the threshold until the crack catches up to the leading one. Thus its propagation is faster than the leading one's. Then, the rear crack slightly bypasses the first and takes the place of the leading one in the previous discussion. This whole procedure of competition between the increase in stored energy due to drying and the phase of unloading/loading due to the geometry is repeated, leading to alternating patterns.

The crack pattern of our experiments is consistent with the above-described model. First, the upward propagation of the cracks is the signature of the upward formation of a gel adhering to the tube wall, in which fracture occurs. By gel, we mean, according to Brinker and Scherer,[16] the formation of a spanning cluster across the section of the tube in which elasticity appears by the creation of a solid network. Second, the wavelength evolution of the crack is coherent with the proposed mechanisms. Indeed, as the compaction front grows up, the pressure gradient decreases (Figure 4.3). Hence, the distance between the same pressure conditions increases so that the distance between similar fracture initiation conditions increases, leading to an increasing wavelength as the leading crack progresses (Figure 3). However, at long time, secondary cracks (one of such a crack can be guessed in Figure 2a) appear and are perpendicular to the tube axis. They generate new air−gel interfaces submitted to capillary pressure P_c so that the pressure is now $P(z) \approx P_c(z_F - z)(z_F - z_l)$. Therefore, the pressure difference acts over a shorter distance, and the pressure gradient increases abruptly (Figure 4.4). This explains that the wavelength decreases when a secondary crack appears (Figure 3). The inset of Figure 3 presents the evolution of the wavelength as a function of the distance to the secondary cracks (new interfaces), showing that, between two decreases in Figure 3, the wavelength increases linearly, with the same slope, as the compaction front rises that is the cracks grow up, in agreement with the previous picture.

To assess the model fully, further experimental investigations and numerical calculations are necessary. In particular, the influences of the diameter of the tube and of the suspension used (solvant and particules[10−12,14]) have to be studied. The compaction front also has to be visualized. Unfortunately, probably because of the geometry of the tube, it cannot simply be observed as in the drying experiments in flat tubes.[13−15] The brittle fracture mechanics proposed model has to be assessed by fully 3D finite element calculations[19] of the mechanical fields (displacements and stresses) of the problem. All of these developments are under study and will be the subject of another paper but are beyond the scope of this letter, which is mainly to present a new self-organized fracture pattern.

Conclusions

Crack dynamics have been investigated in 3D geometry. The arrangement of cracks reveals a self-organized structure consisting of two cracks taking place in two perpendicular planes. The dynamics of these cracks exhibit the alternating propagation of a slow and a fast crack, and this dynamics leads to a band structure of alternating rough and smooth regions. This may explain the alternating rough and smooth face formation in basaltic columnar joints.[5] In this letter, attention has been focused on the description of the peculiar macroscopic fast and slow, smooth and rough aspects of the dynamics of fracture obtained in this 3D drying geometry. It has been shown that the observations can be interpreted using the picture of drying and cracking driven by capillary pressure on the air−gel interfaces proposed by Dufresne et al.[14] in 2D geometry and linear elastic fracture mechanics arguments. Nevertheless, further experimental and theoretical investigations are necessary to quantitatively assess and complete this picture.

Acknowledgment. We thank C. Allain, H. Auradou, P. Gondret, and D. Salin for useful discussions.

LA063702W